Probing top-quark couplings indirectly at Higgs factories [*]

Gauthier Durieux[1;1)]   Jiayin Gu(顾嘉荫)[2;2)]   Eleni Vryonidou[3;3)]   Cen Zhang(张岑)[4;4)]

[1] DESY Notkestraße 85, D-22607, Hamburg, Germany
[2] PRISMA Cluster of Excellence, Institut für Physik,
Johannes Gutenberg-Universität, 55099 Mainz, Germany
[3] Theoretical Physics Department, CERN, 1211 Geneva 23, Switzerland
[4] Institute of High Energy Physics, and School of Physical Sciences,
University of Chinese Academy of Sciences, Beijing 100049, China

Abstract: We perform a global effective-field-theory analysis to assess the combined precision of Higgs couplings, triple gauge-boson couplings, and top-quark couplings, at future circular e^+e^- colliders, with a focus on runs below the $t\bar{t}$ production threshold. Deviations in the top-quark sector entering as one-loop corrections are consistently taken into account in the Higgs and diboson processes. We find that future lepton colliders running at center-of-mass energies below the $t\bar{t}$ production threshold can still provide useful information on top-quark couplings, by measuring virtual top-quark effects. With rate and differential measurements, the indirect individual sensitivity achievable is better than at the high-luminosity LHC. However, strong correlations between the extracted top-quark and Higgs couplings are also present and lead to much weaker global constraints on top-quark couplings. This implies that a direct probe of top-quark couplings above the $t\bar{t}$ production threshold is also helpful for the determination of Higgs and triple-gauge-boson couplings. In addition, we find that below the $e^+e^- \to t\bar{t}h$ production threshold, the top-quark Yukawa coupling can be determined by its loop corrections to all Higgs production and decay channels. Degeneracy with the ggh coupling can be resolved, and even a global limit is competitive with the prospects of a linear collider above the threshold. This provides an additional means of determining the top-quark Yukawa coupling indirectly at lepton colliders.

1 Introduction

After the discovery of the Higgs boson [1, 2], understanding the electroweak symmetry breaking mechanism remains one of the major challenges in particle physics. The determination of Higgs couplings at the Large Hadron Collider (LHC) is now approaching, and in some cases surpassing, the 10% precision level. Improvements beyond this level can be foreseen at proposed e^+e^- colliders. These machines could run at a center-of-mass energy of 240–250 GeV—where the maximum of the $e^+e^- \to hZ$ cross section lies—or even above, and would provide a much cleaner environment for precision determination of Higgs couplings. Prospects have been widely studied through global analyses in the Standard Model effective field theory (SMEFT) and revealed that improvements of up to several orders of magnitude can be achieved compared to present limits [3–9].

Given the expected precision of measurements at future lepton colliders, next-to-leading-order (NLO) theory predictions in the SMEFT can potentially be relevant. These corrections can involve effective operators which do not appear at leading order, and therefore provide new opportunities in the exploration of physics beyond the Standard Model (SM). For instance, the indirect determination of the trilinear Higgs self-coupling, which enters single Higgs production and decay processes at one-loop level, has already been studied [8–10].

  1) E-mail: gauthier.durieux@desy.de
  2) E-mail: jiagu@uni-mainz.de
  3) E-mail: eleni.vryonidou@cern.ch
  4) E-mail: cenzhang@ihep.ac.cn

Effective operators which give rise to anomalous tbW, ttZ, $tt\gamma$ and tth couplings of the top quark can also become relevant at one-loop level. If future lepton colliders run above the $e^+e^- \to t\bar{t}$ and $t\bar{t}h$ production thresholds, these operator coefficients will be determined by direct measurements (see Ref. [11] for a recent global study of top-quark operators at future lepton colliders). Yet, at lower center-of-mass energies, they enter in loop corrections to other electroweak processes. Recently, it has been pointed out that these corrections are already non-negligible at the LHC [12]. Runs of future lepton colliders below the $t\bar{t}$ and $t\bar{t}h$ production thresholds may thus still provide complementary information on top-quark couplings.

Moreover, the top quark is an indispensable player in Higgs coupling analyses, due to its large Yukawa coupling. Already in the SM, several important channels are dominated by its loop contributions. Deviations which would be observed there could be caused by the anomalous top-quark couplings. However, it has been stressed in Ref. [5] that NLO SMEFT predictions for processes that are not loop-induced in the SM are necessary for a global and consistent fit at that order. Fortunately, computations at NLO in the electroweak gauge couplings have become available for Higgs processes in the past few years [13–21]. In particular, the NLO corrections involving top-quark operators for Higgs processes have become available very recently [12], making such a combined analysis feasible at future lepton colliders. The only missing ingredient was the theory prediction for W^+W^- production at the same order. This process is notably sensitive to the triple gauge-boson couplings (TGC) which can be generated by operators which also affect Higgs interactions.

In this work, we extend the theory calculation and implementation of Ref. [12] with the one-loop contributions of top-quark operators to the $e^+e^- \to W^+W^-$ process. This allows us to perform a consistent global fit in the SMEFT, with Higgs couplings and TGCs at the tree level and top-quark operators at the one-loop level. Our main focus is on future circular lepton colliders with very good Higgs measurements but center-of-mass energies not large enough to reach the $t\bar{t}$ or $t\bar{t}h$ production thresholds. We aim to answer the following questions:

- If future lepton colliders only run below the $t\bar{t}$ ($t\bar{t}h$) threshold, can they still determine top-quark–gauge-boson (top-quark Yukawa) couplings with high precision?

- Does the uncertainty on top-quark couplings affect the reach of future measurements of Higgs couplings?

The paper is organized as follows. In Section **2**, we describe our theoretical framework. In Section **3**, we review the calculation and implementation of Ref. [12], and extend it to include $e^+e^- \to W^+W^-$ production. In Section **4**, we describe the measurements and the fit. We discuss our results in Section **5** before concluding in Section **6**. The likelihood of our fits are provided in an ancillary associated with our arXiv preprint.

2 Effective field theory framework

In the absence of clear signs of physics beyond the Standard Model (BSM), a common approach for testing the SM and identifying possible deviations is provided by the SMEFT [22–24]. BSM effects are captured by a series of higher dimensional operators whose coefficients can be related to the parameters of specific models by a matching calculation. Given that all the operators of odd dimension violate baryon or lepton numbers [25], the most important deviations are expected to be captured by operators of dimension six:

$$\mathcal{L}_{\text{EFT}} = \mathcal{L}_{\text{SM}} + \sum_i \frac{C_i}{\Lambda^2} O_i^{(6)} + \dots \qquad (1)$$

Measurements at the LHC and future lepton colliders can be conveniently interpreted in terms of their coefficients.

Two features of the SMEFT are of particular relevance to this work. The first is that theory predictions can be improved systematically, order by order. The SMEFT is a theory that is renormalizable order by order in $1/\Lambda^2$ [26]. Thus, theory predictions can always be improved to match experimental uncertainties. This is one of the main advantages of the SMEFT over other BSM parametrizations, such as the anomalous coupling approach to top-quark couplings, and the κ framework for Higgs couplings.

The second feature is that the SMEFT gives unambiguous and model-independent results only if all operators up to a given dimension and up to a given loop order are included simultaneously. This motivates the inclusion of top-quark operators at the one-loop level in all Higgs and diboson processes entering our global analysis and not only in loop-induced ones like $h \to gg$, $\gamma\gamma$ or $Z\gamma$. In doing so, we include the contribution of each operator considered at its leading order, i.e. at tree level for Higgs operators, and at one-loop level for most top-quark operators. The tree- and loop-level contributions of other operators are not considered. This may be justified either from a bottom-up or from a top-down point of view. Without imposing restrictions on the type of BSM model covered by our SMEFT, one may argue that other operators are sufficiently constrained by measurements different from the ones considered here. One may also argue that the class of models which would dominantly affect the top-quark and Higgs couplings through the operators we consider is worth studying.

Four-fermion operators giving rise to $e^+e^-t\bar{t}$ contact interactions are also disregarded, although they could potentially play a role. They contribute to Higgs and electroweak processes once the top-quark line is closed in a loop. In particular, the two-fermion and the four-fermion operators cannot be efficiently discriminated if $e^+e^- \to t\bar{t}$ is only measured near threshold [11]. So, without higher energy runs, the Higgs and diboson measurements could potentially be used to break this degeneracy. Therefore, the inclusion of these operators could affect our results. However, these corrections have not been computed so far and would affect the renormalization of other SMEFT operators. The implementation of the one-loop contributions of four-fermion operators, as well as a full analysis of their impact, are therefore left to future study. As these four-fermion operators are included in the global tree-level analysis of Ref. [11], we set their coefficients to zero when using results from there.

Our global analysis of Higgs and diboson measurements is based on that of Ref. [5]. Various observables are combined to constrain efficiently all directions of the multidimensional space spanned by the Higgs and top-quark operator coefficients. They will be discussed in Section **4**. We work under the same assumptions: departing from flavor universality only to single out top-quark operators and distinguish the various measurable Yukawa couplings, as well as taking electroweak and CP-violating observables to be perfectly SM-like[1]. We also neglect the quadratic contributions of dimension-six operators as justified in Ref. [5]. Operators that modify Higgs couplings and TGCs are then captured by the following 12 parameters of the Higgs basis:

$$\begin{aligned} &\delta c_Z, \quad c_{ZZ}, \quad c_{Z\square}, \quad \bar{c}_{\gamma\gamma}, \quad \bar{c}_{Z\gamma}, \quad \bar{c}_{gg}, \\ &\delta y_t, \quad \delta y_c, \quad \delta y_b, \quad \delta y_\tau, \quad \delta y_\mu, \quad \lambda_Z. \end{aligned} \tag{2}$$

As described in Ref. [5] (with different notations), they can be easily mapped to the coefficients of 12 SILH-like basis operators:

$$\begin{aligned} &O_{\varphi W} = \varphi^\dagger \varphi W_{\mu\nu}^I W^{I\mu\nu}, &&O_{\varphi B} = \varphi^\dagger \varphi B_{\mu\nu} B^{\mu\nu}, \\ &O_{\varphi\square} = (\varphi^\dagger \varphi)\square(\varphi^\dagger \varphi), &&O_W = iD^\mu \varphi^\dagger \tau^I D^\nu \varphi W_{\mu\nu}^I, \\ &O_B = iD^\mu \varphi^\dagger D^\nu \varphi B_{\mu\nu}, &&O_{b\varphi} = (\varphi^\dagger \varphi)\bar{Q}b\varphi + h.c., \\ &O_{\mu\varphi} = (\varphi^\dagger \varphi)\bar{l}_2 e_2 \varphi + h.c., &&O_{\tau\varphi} = (\varphi^\dagger \varphi)\bar{l}_3 e_3 \varphi + h.c., \\ &O_{t\varphi} = (\varphi^\dagger \varphi)\bar{Q}t\tilde{\varphi} + h.c., &&O_{c\varphi} = (\varphi^\dagger \varphi)\bar{q}_2 u_2 \tilde{\varphi} + h.c., \\ &O_{WWW} = \epsilon^{IJK} W_\mu^{I\nu} W_\nu^{J\rho} W_\rho^{K\mu}, &&O_{\varphi G} = \varphi^\dagger \varphi G_{\mu\nu} G^{\mu\nu}, \end{aligned} \tag{3}$$

where Q is the third-generation quark doublet. The subscripts 2, 3 are flavor indexes (weak and mass eigenstate fermions are not distinguished, approximating mixing matrixes by the identity). The assumption of perfect

electroweak precision measurements in Ref. [5] allowed disregarding of the two operators

$$O_{\varphi WB} = \varphi^\dagger \tau^I \varphi W_{\mu\nu}^I B^{\mu\nu}, \quad O_{\varphi D} = \left(\varphi^\dagger D^\mu \varphi\right)^* \left(\varphi^\dagger D_\mu \varphi\right). \tag{4}$$

In this work, this assumption must be enforced at the one-loop level, also including top-quark operators. This will be discussed in the next section.

The 14 Higgs operators above form a set consistent with the basis employed in the calculation of Ref. [12]. The top-quark operators considered here are the following:

$$\begin{aligned} O_{t\varphi} &= \bar{Q}t\tilde{\varphi}(\varphi^\dagger \varphi) + h.c., \\ O_{\varphi Q}^{(1)} &= (\varphi^\dagger i\overleftrightarrow{D}_\mu \varphi)(\bar{Q}\gamma^\mu Q), \\ O_{\varphi Q}^{(3)} &= (\varphi^\dagger i\overleftrightarrow{D}_\mu^I \varphi)(\bar{Q}\gamma^\mu \tau^I Q), \\ O_{\varphi t} &= (\varphi^\dagger i\overleftrightarrow{D}_\mu \varphi)(\bar{t}\gamma^\mu t), \\ O_{tW} &= (\bar{Q}\sigma^{\mu\nu}\tau^I t)\tilde{\varphi}W_{\mu\nu}^I + h.c., \\ O_{tB} &= (\bar{Q}\sigma^{\mu\nu}t)\tilde{\varphi}B_{\mu\nu} + h.c., \\ O_{tG} &= (\bar{Q}\sigma^{\mu\nu}T^A t)\tilde{\varphi}G_{\mu\nu}^A + h.c.. \end{aligned} \tag{5}$$

The $O_{\varphi tb}$ operator is neglected because its interferences with SM amplitudes are suppressed by a factor of m_b. In addition, we define

$$O_{\varphi Q}^{(+)} \equiv \frac{1}{2}\left(O_{\varphi Q}^{(1)} + O_{\varphi Q}^{(3)}\right), \quad O_{\varphi Q}^{(-)} \equiv \frac{1}{2}\left(O_{\varphi Q}^{(1)} - O_{\varphi Q}^{(3)}\right), \tag{6}$$

and exclude $O_{\varphi Q}^{(+)}$, which affects the tightly constrained $Z \to b\bar{b}$ branching fraction and asymmetry. Note that $O_{t\varphi}$ has already been included in the Higgs operators, and its coefficient has a simple relation with δy_t[2]:

$$\delta y_t = -\frac{C_{t\varphi} v^2}{\Lambda^2}. \tag{7}$$

In summary, the following 6 top-quark operator coefficients are included in our analysis:

$$C_{\varphi t}, \quad C_{\varphi Q}^{(-)}, \quad C_{tW}, \quad C_{tB}, \quad C_{t\varphi}, \quad C_{tG}. \tag{8}$$

Apart from the top-quark operators, loop corrections also provide new opportunities for indirectly constraining the Higgs trilinear coupling, λ_3. The modification in this coupling is induced by a dimension-six operator $O_\varphi = (\varphi^\dagger \varphi)^3$. The coupling can be directly constrained at the LHC, but only at the $\mathcal{O}(1)$ level even assuming the high luminosity scenario [29]. It was shown in Ref. [10] that the measurements of the Higgsstrahlung process at lepton colliders can have an indirect but competitive reach on this coupling via its loop contribution. A global analysis was performed in Ref. [8], which showed that the discrimination between the Higgs trilinear coupling and other Higgs operators is possible, but nevertheless nontrivial. In this work, to determine the impact

---

1) For studies concerning CP-violating top-Higgs interactions at future Higgs factories, see Refs. [27, 28].

2) δy_t receives an additional contribution from $C_{\varphi\square}$. It is omitted because δy_t in our calculation enters at the loop level, while we only aim at the LO contribution from $C_{\varphi\square}$.

of λ_3 on the global reach of the top-quark operators, we follow Ref. [8] and include its one-loop contribution to all the single Higgs processes, parameterized by $\delta\kappa_\lambda \equiv \kappa_\lambda - 1$, where κ_λ is the ratio of the Higgs trilinear coupling to its SM value,

$$\kappa_\lambda \equiv \frac{\lambda_3}{\lambda_3^{\mathrm{SM}}}, \qquad \lambda_3^{\mathrm{SM}} = \frac{m_h^2}{2v^2}. \qquad (9)$$

By turning this coupling on and off in our fit, we will see how much the determination of top-quark couplings is affected.

3   Theory predictions

To the precision needed for this work, the theory predictions for, e.g., total cross sections can be written as

$$\sigma = \sigma_{\mathrm{SM}} + C_h(\mu_{\mathrm{EFT}})\sigma_{\mathrm{tree}}$$
$$+ C_t(\mu_{\mathrm{EFT}})\frac{\alpha_{\mathrm{EW}}}{\pi}\left(\sigma_{\log}\log\frac{Q^2}{\mu_{\mathrm{EFT}}^2} + \sigma_{\mathrm{fin}}\right). \qquad (10)$$

Here, $C_h(\mu_{\mathrm{EFT}})$ is the coefficient of some Higgs or TGC operator O_h that contributes at the tree level, and μ_{EFT} is the scale at which the coefficient is defined. In this work we take $\mu_{\mathrm{EFT}} = m_H$ for all measurements. C_t is the coefficient of some top-quark operator O_t which enters at the loop level and could potentially mix into O_h. Q^2 is the scale of the process. The calculation of σ_{tree} is straightforward, while $\sigma_{\log}$ can be obtained from the running of SMEFT coefficients. In this section, we review the computation of the genuine electroweak corrections σ_{fin} carried out in Ref. [12] for Higgs processes. We then compute them for $e^+e^- \to W^+W^-$ production.

The complete set of electroweak NLO corrections to precision electroweak operators from top-quark operators was first given in Ref. [30]. Results can conveniently be obtained in the "star scheme" [31], because all contributions are oblique. For Higgs production this is no longer the case. In addition to the VV self-energy corrections one also has to compute hh and hVV functions, where V is a photon, W or Z boson. While several calculations were available in the previous literature [13–16, 18–20], the complete results for top-quark operator contributions to Higgs production in the Vh and VBF channels, as well as decay modes $h \to \gamma\gamma, \gamma Z, Wl\nu, Zll, b\bar{b}, \mu\mu, \tau\tau$, were first presented in Ref. [12]. This excludes the four-fermion operators mentioned previously. The calculation is implemented in the MadGraph5_aMC@NLO framework [32], whose reweighting functionality [33] is used to compute the dimension-six top- and bottom-quark loop contributions. The SM parameters are renormalized consistently in the m_W, m_Z and G_F scheme up to dimension six, and operator coefficients are renormalized in the $\overline{MS}$ scheme. The rational $R2$ counterterms are computed following the scheme of Ref. [34–36], for ZZ, hh, hVV, ffV and

ffh loop functions. The implementation provides an automatic and convenient way to simulate indirect contributions from top-quark operators, which enter Higgs processes as NLO electroweak corrections. Events can be generated and matched to parton shower, allowing for detailed investigations using the full differential information.

In the SMEFT formalism, the measurements of Higgs couplings and TGCs are entangled [37–39]. W pair production is therefore an important component of global Higgs analyses at future lepton colliders. For this reason, we extend the calculation of Ref. [12] to incorporate the $e^+e^- \to W^+W^-$ process. Some diagrams involving dimension-six operators are shown in Fig. 1. Additional counterterms need to be computed for the $WW\gamma$ and WWZ vertexes. Among the three TGC operators, only O_W and O_B are renormalized by top-quark operators. The anomalous dimensions are derived in Ref. [12]. Another difficulty is that the $WW\gamma$ function involves a triangle anomaly diagram. In our scheme, this implies that the $R2$ counterterms depend on the choice of the vertex from which the trace of the fermion loop starts. This effect is in principle cancelled by a Wess-Zumino term generated when chiral fermions in the full theory are integrated out [40]. The problem can be fixed by imposing the Ward identity of the photon in the low-energy effective theory. We provide more details in Appendix A. We have validated our implementation of the $WW\gamma$ vertex by computing processes with an external photon and checking that the Ward identity is satisfied.
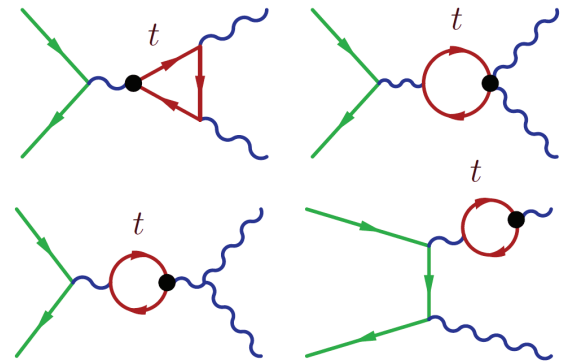

Fig. 1. (color online) Selected diagrams for dimension-six top-quark contributions to $e^+e^- \to W^+W^-$. The red lines represent the top quark, and the blobs represent dimension-six operator insertions.

Our global analysis relies on the assumption that precision electroweak measurements are perfectly constrained to be SM-like. This has consequences on our renormalization scheme, as explained in the following.

In our operator basis, precision electroweak observables receive tree-level contributions from $O_{\varphi WB}$ and $O_{\varphi D}$ operators. At that order, their coefficients are thus simply removed from the fit by assuming the measurements of precision electroweak observables perfectly match SM predictions. Top-quark operators, however, start contributing at the loop level. In the $\overline{MS}$ scheme, the same assumption implies that $C_{\varphi WB}$ and $C_{\varphi D}$ need to take specific values to cancel these loop corrections. These nonzero values will then in turn modify other Higgs production and decay channels, making the fit more complicated. In Ref. [12], a more convenient approach has been followed, where $C_{\varphi WB}$ and $C_{\varphi D}$ are defined in the on-shell scheme using oblique parameters as renormalization conditions. Therefore, if the oblique parameters are tightly constrained, we can exclude $C_{\varphi WB}$ and $C_{\varphi D}$ from the fit.

Instead of using oblique parameters, we further refine this approach in this work, by using the full set of Z-pole and W-pole measurements listed in Ref. [41] as

our renormalization conditions. We assume that, apart from deviations in the top-quark and the Yukawa sectors, BSM effects are otherwise universal, in the sense that they can be captured by dimension-six operators which involve SM bosons only, up to suitable field redefinitions [42]. Their effects in Higgs, WW, and Z/W-pole measurements are then fully captured by the operators listed in Section **2**[1]). With this assumption, the two most constraining degrees of freedom from Z-pole and W-pole measurements can then be used as physical observables to renormalize the coefficients of the $O_{\varphi WB}$ and $O_{\varphi D}$ operators. In the following, we briefly describe the procedure.

According to Ref. [30], contributions from dimension-six top-quark operators to precision electroweak measurements can be conveniently evaluated in the α, m_Z and G_F scheme, by taking the SM tree-level predictions at the Z pole, written in terms of α, m_Z and s_W, and making the following substitutions:

$$\alpha \rightarrow \alpha_* = \alpha + \delta\alpha = \alpha\left(1 - \Pi'_{\gamma\gamma}(q^2) + \Pi'_{\gamma\gamma}(0)\right) \times \left[1 - \frac{\mathrm{d}}{\mathrm{d}q^2}\Pi_{ZZ}(q^2)|_{q^2=m_Z^2} + \Pi'_{\gamma\gamma}(q^2) + \frac{c_W^2 - s_W^2}{s_W c_W}\Pi'_{\gamma Z}(q^2)\right], \tag{11}$$

$$m_Z^2 \rightarrow m_{Z*}^2 = m_Z^2 + \delta m_Z^2 = m_Z^2 + \Pi_{ZZ}(m_Z^2) - \Pi_{ZZ}(q^2) + (q^2 - m_Z^2)\frac{\mathrm{d}}{\mathrm{d}q^2}\Pi_{ZZ}(q^2)|_{q^2=m_Z^2}, \tag{12}$$

$$s_W^2 \rightarrow s_{W*}^2 = s_W^2 + \delta s_W^2 = s_W^2\left[1 + \frac{c_W}{s_W}\Pi'_{\gamma Z}(q^2) + \frac{c_W^2}{c_W^2 - s_W^2}\left(\Pi'_{\gamma\gamma}(0) + \frac{1}{m_W^2}\Pi_{WW}(0) - \frac{1}{m_Z^2}\Pi_{ZZ}(m_Z^2)\right)\right], \tag{13}$$

taking $q^2 = m_Z^2$. Here $\Pi_{VV}(q^2)$ is the self-energy correction for the $V = \gamma, W, Z$ gauge boson while $\Pi'_{VV}(q^2) \equiv [\Pi_{VV}(q^2) - \Pi_{VV}(0)]/q^2$. Expressions for these corrections are of order C/Λ^2 and can be found in Ref. [30]. Note that unlike in the calculation for Higgs and WW production, here we use G_F instead of m_W as an input parameter, since theory predictions in Ref. [41] are provided in this scheme.

Z-pole observables consist of various combinations of partial widths and asymmetries. Their SM predictions only depend on s_W and on the product of α and m_Z. Thus, these measurements only constrain two independent combinations of top-quark operator coefficients. The correction to the W mass can be written as

$$\frac{\delta m_W^2}{m_W^2} = \frac{s_W^2}{c_W^2 - s_W^2}\Pi'_{\gamma\gamma}(0) + \frac{c_W^2}{c_W^2 - s_W^2}\frac{1}{m_W^2}\Pi_{WW}(0) - \frac{c_W^2}{c_W^2 - s_W^2}\frac{1}{m_Z^2}\Pi_{ZZ}(m_Z^2) + \Pi'_{WW}(m_W^2), \tag{14}$$

and constitutes the third independent combination constrained. Finally, the width of the W boson is corrected

by

$$\delta\left(\frac{\Gamma_W}{m_W}\right)^2 = \left(\frac{\Gamma_W}{m_W}\right)^2 \times \left(\frac{\delta m_W^2}{m_W^2} - \Pi'_{WW}(m_W^2) + \frac{\mathrm{d}}{\mathrm{d}q^2}\Pi_{WW}(q^2)|_{q^2=m_W^2}\right), \tag{15}$$

which is almost degenerate with the previous constraint. Given the relatively weaker precision on the measurement of Γ_W and the approximate degeneracy, we expect this fourth constraint to be less useful.

We now modify the renormalization of $C_{\varphi\mathrm{WB}}$ and $C_{\varphi D}$ by finite Δ_{ij} constants, so that

$$C_i \Rightarrow Z_{ij}C_j = C_i + \delta Z_{ij}C_j, \tag{16}$$

$$\delta Z_{ij} = \frac{\alpha}{2\pi}\Gamma(1+\epsilon)\left(\frac{4\pi\mu^2}{\mu_{\mathrm{EFT}}^2}\right)^\epsilon\left(\frac{1}{\epsilon} + \Delta_{ij}\right)\gamma_{ij}, \tag{17}$$

for $O_i = O_{\varphi\mathrm{WB}}, O_{\varphi D}$. The O_j cover all top-quark operators. We then need to choose the values of Δ_{ij} which minimize the deviations in the precision observables when setting $C_{\varphi\mathrm{WB}} = C_{\varphi D} = 0$. To find them, we construct a χ^2 using the experimental results and theory predictions for all W and Z pole data listed in

---

1) In the SILH basis, two additional operators $O_{2B} = -\frac{1}{2}(\partial^\mu B_{\mu\nu})^2$ and $O_{2W} = -\frac{1}{2}(D^\mu W_{\mu\nu}^a)^2$ are universal, but they can be eliminated in favor of four-fermion operators, and thus drop out from the pole measurements.

Ref. [41]. The associated covariance matrix has four positive eigenvalues, corresponding to the four independent constraints expected. The Δ_{ij} are chosen such that the two most constrained eigenvectors only involve $C_{\varphi\mathrm{WB}}$ and $C_{\varphi D}$:

$$+0.906C_{\varphi\mathrm{WB}}+0.423C_{\varphi D}=0\pm0.0000234 \qquad (18)$$

$$-0.423C_{\varphi\mathrm{WB}}+0.906C_{\varphi D}=0\pm0.0124, \qquad (19)$$

for $\Lambda = 1$ TeV. In this specific scheme and up to one-loop order, the two most stringent limits from Z- and W-pole data only constrain the renormalized $C_{\varphi\mathrm{WB}}$ and $C_{\varphi D}$ to small values. The assumption of perfect precision measurements approximates these two limits to be infinitely constraining and allows us to exclude $C_{\varphi\mathrm{WB}}$ and $C_{\varphi D}$ from the rest of our analysis at the one-loop level. This can be interpreted as using the first two degrees of freedom of the precision measurements as on-shell renormalization conditions for these two coefficients.

There are two remaining constraints. One is associated with a covariance matrix eigenvalue of about 300 TeV^{-2}, and is the weakest. We therefore ignore it. The other implies $0.17C_{\varphi Q}^{(-)}-0.10C_{\varphi t}-0.04C_{tB}-0.92C_{tW}=0\pm0.60\times(\Lambda/\mathrm{TeV})^2$ and involves only top-quark operators. We include this constraint in our fit, conservatively assuming that it could be strengthened by a factor of five with future lepton collider data. Our final results are, however, largely insensitive to this constraint.

The above renormalization scheme, as well as the W-pair process are then supplemented to the UFO model described in Ref. [12]. It allows for the automatic calculations of all Higgs and W-pair processes relevant to this work. Beside inclusive cross sections, differential distributions can also be obtained. The production angle in $e^+e^- \to W^+W^-$ will be used in our analysis.

Our discussion so far has excluded the top-quark chromo-dipole operator O_{tG}. It enters $h \to gg$ through a top-quark loop which has already been studied in the literature [43, 44]. This effect will be included in our global analysis.

4   Measurements and fit

In this section, we describe the measurements and observables used in our analysis. Since our study is most relevant for lepton colliders with very good Higgs measurements but not large enough center-of-mass energies to reach the $t\bar{t}$ or $t\bar{t}h$ production thresholds, our primary focus will be on the circular colliders. Currently, two proposals for such colliders have been made: the Circular Electron Positron Collider (CEPC) in China [45], and the Future Circular Collider with e^+e^- beams (FCC-ee) at CERN [46]. In this study, we consider the following hypothetical scenario: a circular collider (CC) collecting an integrated luminosity of 5 ab^{-1} at a center-of-mass

energy of 240 GeV and possibly also running at the top-quark pair production threshold with 0.2 ab^{-1} gathered at 350 GeV and 1.5 ab^{-1} at 365 GeV. The incoming electron and positron beams are assumed to be unpolarized. This scenario closely follows the current projected run plan of the FCC-ee [47]. The 350 and 365 GeV runs could fix the top-quark electroweak couplings by directly probing $t\bar{t}$ production, though approximate degeneracies would remain due to limited energy lever arm. The top-quark Yukawa coupling, on the other hand, cannot be directly probed in such a run scenario. We will also show results with only a 240 GeV run, which represents the CEPC scenario. At the moment, there is no plan for the CEPC to run at center-of-mass energies beyond 240 GeV, though a future upgrade to the top-quark pair production threshold remains an open possibility. Our study could then provide useful information regarding the impact of a 350 GeV upgrade on the measurements of the top-quark couplings and on the indirect effect of their loop contributions on Higgs coupling determinations. Both CEPC and FCC-ee plan to also run at the Z-pole and WW production threshold, which could significantly improve the sensitivities on the electroweak observables that are already tightly constrained by LEP measurements.

Linear colliders, such as the Compact Linear Collider at CERN [48] and the International Linear Collider [49], could run at higher energies and, in particular, above the thresholds for both $t\bar{t}$ and $t\bar{t}h$ productions. With these measurements, the top-quark operators can be probed at the tree level, with a sensitivity far better than the current one. Although information about top-quark couplings may only be indirectly available at the first 250 GeV stage of the ILC, we will not treat this case explicitly and will not further consider linear collider scenarios.

Table 1.   Estimates for the precision reachable on key top-quark observables at the HL-LHC.

channels	uncertainties	
	without th. unc.	with th. unc.
$t\bar{t}$	4% [50]	7%
single top (t-ch.)	4% [51]	4%
W-helicity (F_0)	3% [52]	3%
W-helicity (F_L)	5% [52]	5%
$t\bar{t}Z$	10%	15%
$t\bar{t}\gamma$	10%	17%
$t\bar{t}h$	10%	16% [53]
$gg \to h$	4%	11% [53]

The HL-LHC measurements could provide important complementary information. To the best of our knowledge, a systematic determination of the projected sensitivity to top-quark couplings is unfortunately not available in the literature. We therefore consider the measurements in Table 1 and estimate the precision reachable

with the HL-LHC. Here, the projected precisions on measurements of the $t\bar{t}$ and t-channel single top-quark production cross sections and W-helicity in top-quark decay are based on the works referred to. Theoretical uncertainties for single top-quark production and W-helicity measurements are neglected, as they are both of order $\mathcal{O}(1\%)$ [54, 55]. The uncertainties on $t\bar{t}h$ and $gg \to h$ production cross sections are taken from Ref. [53]. The ones imposed on the $t\bar{t}Z/\gamma$ cross sections are simple estimates. Theoretical uncertainties are estimated from predictions at NLO in QCD. A combination of $t\bar{t}$, $t\bar{t}h$ and $gg \to h$ production cross section measurements is sufficient to constrain O_{tG}, $O_{t\varphi}$ and $O_{\varphi G}$ ($\bar{c}_{gg}$). The W-helicity measurements alone fix O_{tW}. The remaining three operators, $O_{\varphi t}$, $O_{\varphi Q}^{(-)}$ and O_{tB}, are constrained by $t\bar{t}Z/\gamma$ and single top-quark production cross section measurements. For the trilinear Higgs self-coupling, we follow Refs. [56, 57] and assume that a constraint of $-0.9 < \delta\kappa_\lambda < 1.3$ at the $\Delta\chi^2 = 1$ level could be obtained at the HL-LHC by measuring both the rate and the distributions of the double Higgs production process. While a global fit should in principle also be performed for the HL-LHC, it was shown in Ref. [56] that the reach on the trilinear Higgs coupling is dominated by the measurement of the double Higgs production, while the other Higgs operators are well constrained by the single Higgs processes and have little impact on the extraction of the trilinear Higgs coupling. We expect this to hold even with the inclusion of top-quark operator contributions in the loops. The combination of measurements in Table 1 with that of double Higgs production captures the most important information on top-quark operators and the trilinear Higgs self-coupling at the HL-LHC.

For the Higgs measurements at lepton colliders, we follow closely the treatment of Ref. [5] and include both the inclusive $e^+e^- \to hZ$ cross section and exclusive Higgs decay channels, as well as the measurement of the WW-fusion production channel, $e^+e^- \to \nu\bar{\nu}h$. The run scenario in Ref. [5] has been updated to the one detailed above. While the differential observables in $e^+e^- \to hZ$ could provide additional information [58, 59], they are not included in our analysis. For these observables, corrections in production and decay of the Higgs and Z need to be simulated simultaneously, and this is not yet possible in our setup. For the diboson production process, $e^+e^- \to W^+W^-$, we consider only the semileptonic decay channel, assuming the statistical uncertainties dominate. In contrast with Ref. [5], we only include the differential distributions of the W-production polar angle. Finally, for the measurements of $t\bar{t}$ production at center-of-mass energies of 350 and 365 GeV, we use the results of Ref. [11]. We do not consider the one-loop corrections to $e^+e^- \to t\bar{t}$ from the top-quark operators, since most of them enter at tree level and can therefore be tightly constrained. In particular, the loop-level dependence in the top-quark Yukawa and chromo-dipole operators are not accounted for. The total χ^2 is obtained by summing over the χ^2 of all the measurements whose central values are assumed to confirm SM predictions.

It was shown in Ref. [5] that, thanks to the high precision of the measurements at the lepton colliders, it is sufficient to only keep the linear dependencies of the observables on the EFT parameters. We found this statement to hold even with the inclusion of the top-quark operator in loops. However, at the HL-LHC, the cross section for $t\bar{t}$ production in association with a Z boson or photon has a limited sensitivity to the linear contributions of O_{tW} and O_{tB} [60], due to the Lorentz structure of these dipole operators and to accidental cancellations between different initial states. The inclusion of the W-helicity measurement significantly improves the reach on O_{tW} and brings its dependence in the fit back to the linear regime. For O_{tB}, on the other hand, the reach is much worse and is mainly driven by the quadratic terms. The inclusion of these terms would significantly complicate our fitting procedure. Since our focus is on the lepton colliders, we simplify the fit by keeping only the linear terms while adding an extra term by hand to the total χ^2 that corresponds to a standard deviation of 3 TeV^{-2} for C_{tB}/Λ^2, which reproduces the main constraints on O_{tB} from the square contributions to a good approximation.

5   Results

In this section, we present the precision reach obtained by a χ^2 fit to the observables described in the previous section. There are two important aspects in the determination of the indirect reach on the top-quark operators from the Higgs and diboson measurements at lepton colliders. First, the overall measurement sensitivity is assessed by performing individual fits to each parameter of Eq. (8), setting all others to zero. The second aspect concerns the discrimination among top-quark operators, and between the Higgs and top-quark operators. Differential information is then crucial to constrain all directions of the SMEFT parameter space with a limited number of processes. Runs at different center-of-mass energies and with different polarizations also help to set meaningful constraints with lepton collider data only, though the latter information is not available at circular colliders. One can otherwise also resort to a combination with HL-LHC measurements.

The individual sensitivities to the top-quark operators of Eq. (8) are shown in Fig. 2 for different measurements at a circular lepton collider as well as at the HL-LHC. The results are presented in terms of the one-sigma reach on C_i/Λ^2, with C_i and Λ defined in Eq. (1).
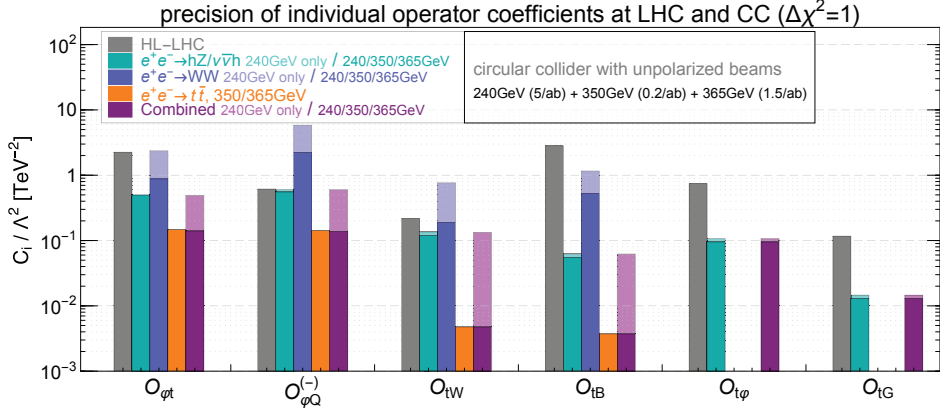
Fig. 2.   (color online) Individual one-sigma reach on top-quark operator coefficients for different future collider scenarios and measurements. One single coefficient is allowed to depart from zero at a time.
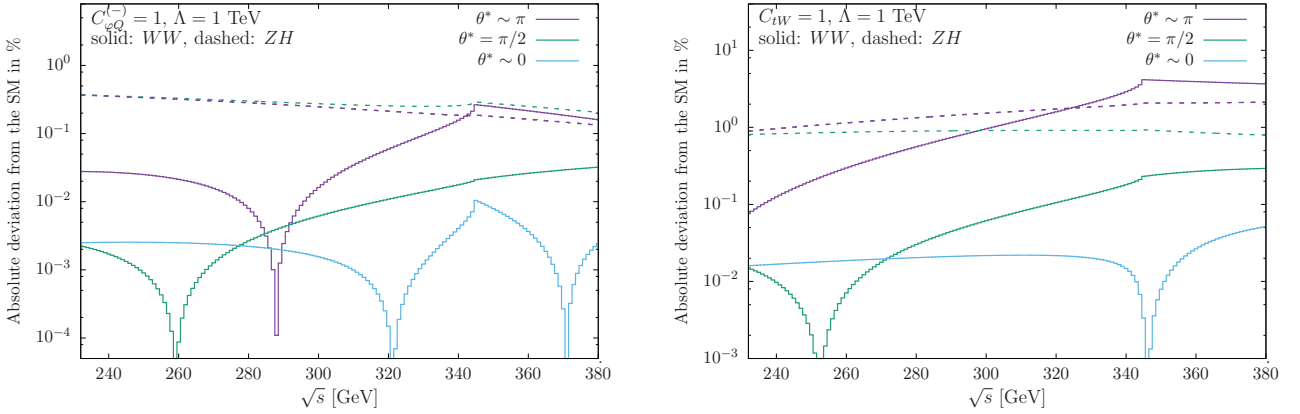

Fig. 3.   (color online) Center-of-mass energy dependence of $O_{\varphi Q}^{(-)}$ (left) and O_{tW} (right) contributions to $e^+e^- \to W^+W^-$ (solid) and Zh (dashed) production, in percentage of the SM rate, for $C/\Lambda^2 = 1$ TeV^{-2}. Dependencies are shown in absolute values (changes of sign generate the visible dips) for three different scattering angles: 0, $\pi/2$ and π. For $e^+e^- \to Zh$, the 0 and π curves overlap.

Five scenarios are considered. The first column corresponds to the HL-LHC measurements listed in Table 1, with theoretical uncertainties included. The second, third and fourth columns respectively include the Higgs, diboson, and $t\bar{t}$ measurements at a circular lepton collider. The last column is obtained from the combination of all these circular collider measurements. Lighter shades are obtained with a 240 GeV run only, while the darker ones combine operation of all three center-of-mass energies considered (240, 350 and 365 GeV).

The indirect individual reach of Higgs and diboson measurements at 240 GeV on top-quark operator coefficients is seen to be better than the direct HL-LHC sensitivity. The loop suppression of top-quark operator contributions is compensated by the high precision of lepton collider measurements. This is one of the main conclusions of this work, and partly answers the first question raised in the introduction. If higher center-of-mass energies are available, direct $e^+e^- \to t\bar{t}$ measurements still provide the best reach on top-quark operators. Note that

the tree-level analysis of the top-quark pair production from Ref. [11] is insensitive to the top-quark Yukawa and chromo-dipole operators. The indirect individual reach of the diboson measurements at 240 GeV is somewhat lower than that of Higgs measurements. However, it improves with 350/365 GeV runs. This higher indirect sensitivity of W pair production to top-quark operators at higher center-of-mass energies is further examined in Fig. 3. For illustration, the contributions of $O_{\varphi Q}^{(-)}$ and O_{tW} operators are shown in percentage of the SM rate, as a function of the center-of-mass energy and for three scattering angles. For comparison, dashed curves show the dependence of $e^+e^- \to Zh$ production.

Among top-quark operators, the improvement brought by 240 GeV Higgs measurements over HL-LHC individual sensitivities is most significant for O_{tB}. It mainly arises from the measurement of the Higgs decay to two photons, $h \to \gamma\gamma$. As shown in Ref. [12], the O_{tB} operator has a particularly large contribution to this decay channel: roughly of the same size as the SM rate
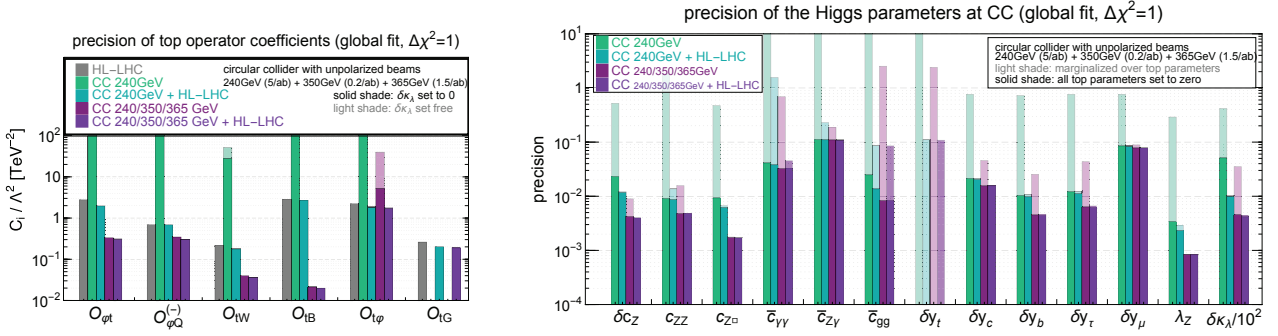
Fig. 4.   (color online) Global one-sigma precision reach on the 18 top-quark (left) and Higgs (right) operator co-
efficients deriving from HL-LHC and circular lepton collider measurements. The Higgs parameter definitions are
those of Ref. [5]. Large degeneracies are present in the CC 240 GeV scenario and push the precision reach on some
operator coefficients to outside the plot range. With lepton-collider measurements only, C_{tG} and $\bar{c}_{gg}$ remain fully
correlated. The constraint displayed for $\bar{c}_{gg}$ is then actually to be interpreted as applying to $\bar{c}_{gg}+0.46C_{tG}$.

when $C_{tB}/\Lambda^2 = (1 \text{ TeV})^{-2}$. On the other hand, no di-
rect measurements at the LHC can probe O_{tB} effi-
ciently. It should be noted that the measurements of $h \rightarrow \gamma\gamma$ at
the HL-LHC could also help in probing O_{tB}. Similarly,
$O_{t\varphi}$ and O_{tG} can be very well constrained individually by
the measurement of $h \rightarrow gg$ at lepton colliders. However,
we will see in our global analysis that the degeneracy
between the top-quark and Higgs operators is to be par-
tially lifted by loop corrections in other Higgs processes.

In Fig. 4, we present the results of the global anal-
ysis for all Higgs and top-quark operator coefficients of
Eq. (2) and (8). It amounts to 18 degrees of freedom once
the trilinear Higgs boson self-coupling is included. Note
that δy_t and $C_{t\varphi}$ represent the same degree of freedom
since they are related through Eq. (7). The reach on
the top-quark and Higgs operator coefficients is shown
in the left-hand and right-hand panels respectively. For
top-quark operators, five scenarios are presented. The
first column shows the reach of the HL-LHC measure-
ments. The second column shows the indirect reach of a
240 GeV run. This result is then combined with the HL-
LHC measurements and displayed in the third column.
The fourth and the fifth columns display similar informa-
tion, but with all three energies, 240, 350 and 365 GeV.
The $e^+e^- \rightarrow t\bar{t}$ measurements are then included. We also
display the impact of $\delta\kappa_\lambda$ on the reach of the top-quark
operators. The results shown with the light shades are
obtained by setting $\delta\kappa_\lambda$ to zero, and the ones with darker
shades are obtained by marginalizing over $\delta\kappa_\lambda$. The im-
pact of $\delta\kappa_\lambda$ is small once the double Higgs measurements
of the HL-LHC are included.

As expected, the indirect global reach of Higgs and di-
boson measurements on top-quark operator coefficients
is much lower than the individual one. In particular,
large degeneracies are present when data from a 240 GeV
run only is exploited, pushing global limits beyond the
range of validity of the EFT. While the dependence of
observables used in the fit on dimension-six operator co-

efficients is still dominated by linear contributions, these
limits should be interpreted with care. The difference
between individual and global constraints is particularly
pronounced for C_{tB}, $C_{t\varphi}$ and C_{tG}, due to their approx-
imate degeneracies with Higgs operators. The $h \rightarrow \gamma\gamma$
branching fraction, for instance, is very well constrained
but, alone, does not discriminate between the contribu-
tions from $C_{t\varphi}$, C_{tB} and $\bar{c}_{\gamma\gamma}$. Similarly, $h \rightarrow gg$ measure-
ments only constrain a combination of $C_{t\varphi}$, C_{tG} and $\bar{c}_{gg}$.
Lepton collider runs nevertheless provide some marginal
improvement in a combination with direct top-quark
measurements at the HL-LHC. Note that the O_{tG} opera-
tor enters $h \rightarrow gg$ but no other measurement at 240 GeV,
so its marginalized limit without combination with HL-
LHC data is absent. At higher energies, it could enter
in NLO corrections to $t\bar{t}$ production (or in $t\bar{t}j$), which
we do not include. This is in contrast with $O_{t\varphi}$, whose
marginalized limit at lepton colliders derive from its loop
corrections to other channels, which are, however, not
loop-induced. We will further discuss the reach on the
top-quark Yukawa coupling at the end of this section.
Direct measurements of $e^+e^- \rightarrow t\bar{t}$ still yield the best
handle on top-quark operator coefficients. As mentioned
earlier, it remains to be examined whether they are also
efficient in indirectly constraining the $O_{t\varphi}$ and O_{tG} op-
erator coefficients in a global analysis. In our treatment,
the main constraints on these parameters arise from the
HL-LHC measurements of $t\bar{t}$, $t\bar{t}h$, and $gg \rightarrow h$.

In the right-hand panel of Fig. 4, the one-sigma reach
on Higgs couplings is presented for circular lepton collid-
ers with and without combination with HL-LHC data.
The impact of a 240 GeV run alone is again separated
from that of the full scenario considered, with operation
at center-of-mass energies of 240, 350 and 365 GeV. In
this figure, we aim to answer the second question raised
in the introduction, by emphasizing the impact of uncer-
tainties on top-quark couplings on the extraction of Higgs
couplings. This is visible in the difference between bars

of lighter and darker shades, for which the corresponding top-quark operator coefficients (including δy_t) are respectively marginalized over or set to zero. Considering a lepton collider run at 240 GeV only, without any direct constraint on top-quark operator coefficients, these uncertainties typically worsen the reach on most Higgs couplings by more than one order of magnitude. Several global limits —on $\bar{c}_{\gamma\gamma}$, $\bar{c}_{Z\gamma}$ and $\bar{c}_{gg}$ in particular— are then too loose to remain meaningful. The impact of the top-quark loop contributions on most Higgs couplings is significantly reduced once direct top-quark pair production measurements are performed above the $e^+e^- \to t\bar{t}$ production threshold. The uncertainty on the top-quark Yukawa coupling still sizeably affects the determination of several Higgs boson couplings. The HL-LHC data cures this issue for all couplings but $\bar{c}_{gg}$. Without a lepton collider run above the $t\bar{t}$ production threshold, the loose constraint on C_{tB} deriving from HL-LHC measurements degrades the global limit on $\bar{c}_{\gamma\gamma}$ by more than one order of magnitude.
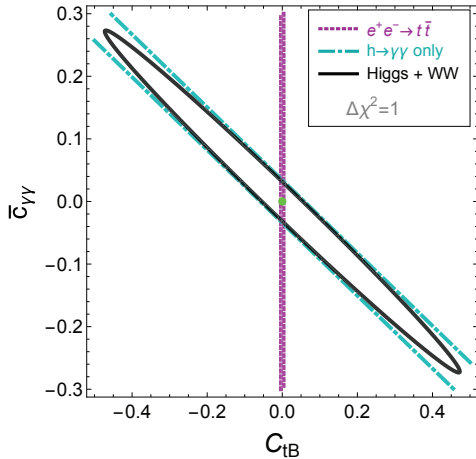

Fig. 5.   (color online) Two-dimensional constraints on C_{tB} and $\bar{c}_{\gamma\gamma}$, with all other parameters set to zero, to illustrate the correlation between Higgs and top-quark couplings.

This correlation is further examined in Fig. 5, showing the individual $\Delta\chi^2 = 1$ sensitivities of various measurements in the two-dimensional parameter space formed by C_{tB} and $\bar{c}_{\gamma\gamma}$. The $h \to \gamma\gamma$ measurement imposes a tight constraint on a linear combination of C_{tB} and $\bar{c}_{\gamma\gamma}$, leading to a strong correlation between these two parameters, but also leaving a blind direction unconstrained. The latter can be lifted either at lepton colliders via loop corrections involving O_{tB} to other processes, or at the HL-LHC via direct ttZ/γ measurements, but none of them is strong enough to simultaneously pin down both couplings. In particular, HL-LHC measurements yield a loose $-2.7 < C_{tB} < 2.1$ constraint for

$\Lambda = 1$ TeV which cannot be displayed in Fig. 5. As already stressed, direct $e^+e^- \to t\bar{t}$ measurements above 350 GeV are needed to resolve this issue. Similar observations can also be made for $\bar{c}_{Z\gamma}$. The lower precision achieved on the $hZ\gamma$ interaction somewhat reduces the impact of correlations in that case.
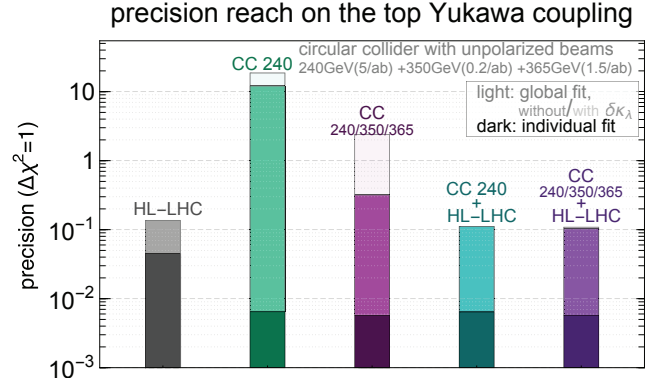

Fig. 6.   (color online) Indirect one-sigma reach on δy_t in different lepton collider scenarios, compared and combined with the HL-LHC measurements.

Finally, we show in Fig. 6 the indirect reach on the top-quark Yukawa coupling, δy_t, from Higgs and diboson measurements at a circular lepton collider. With only a 240 GeV run at a circular lepton collider, a strong correlation with $\bar{c}_{gg}$ makes the global reach on δy_t about three orders of magnitude weaker than the individual one. The individual reach is dominated by the precision of the $h \to gg$ branching fraction measurement (see also Ref. [61]). In contrast, the global reach is determined by loop-level sensitivity of processes that are not loop-induced. Additional runs at center-of-mass energies of 350 and 365 GeV directly fix top-quark–gauge-boson couplings through $e^+e^- \to t\bar{t}$ measurements and improve the global constraint on δy_t by more than an order of magnitude. Still, an approximate degeneracy with the loop-dependence on the trilinear Higgs self-coupling is visible and is only resolved by a combination with HL-LHC measurements[1]. The loop-level sensitivity of $e^+e^- \to t\bar{t}$ on δy_t, which we did not include, is potentially complementary. With a CLIC beam spectrum (broader than that of a circular collider), a $t\bar{t}$ threshold scan alone leads to a precision of about 20% on δy_t, determined simultaneously with the top-quark mass using a total integrated luminosity of 100 fb^{-1} [63]. Setting $\delta\kappa_\lambda$ to zero, the indirect sensitivity of Higgs and diboson processes in runs at center-of-mass energies of 240, 350 and 365 GeV leads to a global one-sigma precision of 32% on δy_t. This reach is competitive with that achievable at the HL-LHC. To compare with direct measurements, the

---

1) Conversely, the impact of the uncertainty on δy_t in the extraction of $\delta\kappa_\lambda$ through loop corrections in $e^+e^- \to hZ$ at 240 GeV was studied in Ref. [62].

$e^-e^+ \to t\bar{t}h$ production cross section with 1 ab^{-1} of integrated luminosity collected at a center-of-mass energy of 500 GeV with a $P(e^+,e^-)=(+0.3,-0.8)$ beam polarization would lead to a precision of 10% on δy_t [64]. We thus conclude that the loop contributions to Higgs and diboson processes studied in this work provide an additional handle on δy_t below the $t\bar{t}h$ threshold, leading to a global reach competitive with that of other direct and/or indirect approaches. This completes the answer to the first question in our introduction.

6   Conclusions

In this work, we have studied the sensitivity of a future circular e^+e^- collider to Higgs couplings, triple gauge-boson couplings, and top-quark couplings. In particular, we focused on runs below the $e^+e^- \to t\bar{t}$ production threshold, where top-quark couplings enter as one-loop corrections. The corrections to the Higgs processes became available in Ref. [12]. We have obtained the corrections to W-boson pair production, which were not previously known. Based on these results, we have performed a global SMEFT analysis including both Higgs and W-pair measurements. This allowed us to derive the future sensitivities to all couplings considered simultaneously.

The main finding of this work is that future lepton colliders running at center-of-mass energies below the $t\bar{t}$ threshold can provide useful information on top-quark couplings through the measurements of virtual effects. The indirect individual sensitivities obtained are higher than the direct HL-LHC ones. Nevertheless, our analysis suggests that an energy upgrade above the $e^+e^- \to t\bar{t}$ production threshold is desirable. On the one hand, the direct individual sensitivity to top-quark couplings is much higher. On the other hand, the strong correlations between the top-quark and Higgs couplings, which manifest themselves in a global analysis, are mitigated. Below the $t\bar{t}$ threshold, global constraints on top-quark couplings are otherwise much weaker than individual ones, if meaningful at all. The combination of a 240 GeV run with direct top-quark coupling measurements at the HL-LHC does not entirely solve this issue. A precise determination of top-quark couplings is thus also crucial for fixing Higgs couplings.

In addition, we find that lepton colliders running below the $t\bar{t}h$ production threshold can also determine the top-quark Yukawa coupling through its loop corrections to other Higgs channels. Combining 240 GeV and 350/365 GeV runs leads to a marginalized limit that is competitive with projected direct limits at the HL-LHC as well as at the ILC with 500 GeV of center-of-mass energy. Higgs and diboson measurements thus provide an alternative indirect determination of the top-quark Yukawa coupling at a future circular lepton collider, beside a $t\bar{t}$ threshold scan. Given that the latter is also affected by the mass of the top quark and the former by loops of the trilinear Higgs self-coupling, the two approaches are expected to be complementary. This interplay should be further studied in the future. Note that the 350/365 GeV runs are crucial for the precision of this approach. This provides another motivation for the corresponding energy upgrade at circular lepton colliders.

A few simplifications have been made throughout our analysis. Four-fermion and CP-odd operators were not included, as the corresponding electroweak NLO corrections are yet not available. Top-quark pair production at lepton colliders was treated at tree level. Precision electroweak measurements were assumed to be infinitely constraining. Our approach could be applied to the lower-energy stages of a linear collider, where beam polarization would provide an additional handle. A more extensive use of differential distributions could also improve the reach we presented here and help to lift approximate degeneracies. Further investigations along these directions can be envisioned.

Appendix A: Gauge anomaly in the $WW\gamma$ vertex

Effective operators could induce gauge anomalies by modifying the top-quark couplings to gauge bosons, which are chiral. In our scheme, this is reflected by the fact that the $R2$ rational counterterms of the $W^+W^-\gamma$ loop function contain a term with the epsilon tensor, whose coefficient depends on the vertex from which we compute the fermionic trace. In the following, we list the epsilon term in the $R2$ counterterms for all relevant operators, with the fermion loop traced from all three vertices, γ, W^+, and W^-. Our convention is that the three external fields, A^μ, $W^{+\nu}$, and $W^{-\rho}$, are associated with

incoming momenta p_1, p_2 and p_3 respectively. They are:

$$O^{(+)}_{\varphi Q}: \quad -\frac{e^3 v^2}{48\pi^2 s_W^2 \Lambda^2} \begin{cases} \epsilon^{\mu\nu\rho\sigma}(p_{2\sigma}-p_{3\sigma}) & \gamma \\ \epsilon^{\mu\nu\rho\sigma}(p_{3\sigma}-p_{1\sigma}) & W^+ \\ \epsilon^{\mu\nu\rho\sigma}(p_{1\sigma}-p_{2\sigma}) & W^- \end{cases} \quad (A1)$$

$$O^{(-)}_{\varphi Q}: \quad \frac{e^3 v^2}{48\pi^2 s_W^2 \Lambda^2} \begin{cases} \epsilon^{\mu\nu\rho\sigma}(p_{2\sigma}-p_{3\sigma}) & \gamma \\ \epsilon^{\mu\nu\rho\sigma}(p_{3\sigma}-p_{1\sigma}) & W^+ \\ \epsilon^{\mu\nu\rho\sigma}(p_{1\sigma}-p_{2\sigma}) & W^- \end{cases} \quad (A2)$$

$$O_{tB}: \quad \frac{3e^2 c_W v m_t}{8\sqrt{2}\pi^2 s_W^2 \Lambda^2} \begin{cases} 0 & \gamma \\ \epsilon^{\mu\nu\rho\sigma} p_{1\sigma} & W^+ \\ -\epsilon^{\mu\nu\rho\sigma} p_{1\sigma} & W^- \end{cases} \quad (A3)$$

$$O_{tW}: \quad \frac{e^2 v m_t}{8\sqrt{2}\pi^2 s_W \Lambda^2} \begin{cases} -3\epsilon^{\mu\nu\rho\sigma}(p_{2\sigma}-p_{3\sigma}) & \gamma \\ 2\epsilon^{\mu\nu\rho\sigma}(p_{1\sigma}-p_{2\sigma}) & W^+ \\ -2\epsilon^{\mu\nu\rho\sigma}(p_{1\sigma}-p_{3\sigma}) & W^- \end{cases} \quad (A4)$$

The field after each line indicates the starting point of the trace. The other operators do not contribute.

This anomaly can be interpreted as the consequence of integrating out heavy chiral fermions. The anomaly-free condition in the UV theory implies anomaly cancellation between different fermions. When matching to the SMEFT, if only some of them are integrated out, the resulting effective field theory could appear to be anomalous. However, when these chiral fermions are integrated out, they also generate a Wess-Zumino term which is supposed to cancel the gauge anomaly in the SMEFT. This term has the following form:

$$c_{\text{WZ}}\frac{e^3}{8\pi^2 s_W^2}\epsilon^{\mu\nu\rho\sigma}A_\mu\left(W_\nu^I\partial_\rho W_\sigma^I+\frac{1}{3}g_W\epsilon_{IJK}W_\nu^I W_\rho^J W_\sigma^K\right). \quad (A5)$$

The coefficient of this term can be determined by requiring that the Ward identity for $U(1)_{\text{EM}}$ is restored in the effective theory. Taking $O^{(+)}_{\varphi Q}$ as an example, we first go to the consistent anomaly [65] by symmetrizing the anomaly with respect to all three external momenta. From Eq. (A1), this corresponds to a vanishing $R2$ counterterm, and

$$p_1^\mu\Gamma_{\mu\nu\rho}=p_2^\mu\Gamma_{\rho\mu\nu}=p_3^\mu\Gamma_{\nu\rho\mu}=-\frac{C^{(+)}_{\varphi Q}e^3 v^2}{48\pi^2 s_W^2 \Lambda^2}\epsilon^{\nu\rho\alpha\beta}p_{2\alpha}p_{3\beta}. \quad (A6)$$

Then, the Wess-Zumino term gives an additional contribution:

$$\Gamma^{\text{WZ}}_{\mu\nu\rho}=c_{\text{WZ}}\frac{e^3}{8\pi^2 s_W^2}\epsilon^{\mu\nu\rho\sigma}(p_{2\sigma}-p_{3\sigma}), \quad (A7)$$

$$p_1^\mu\Gamma^{\text{WZ}}_{\mu\nu\rho}=2c_{\text{WZ}}\frac{e^3}{8\pi^2 s_W^2}\epsilon^{\mu\nu\alpha\beta}p_{2\alpha}p_{3\beta}. \quad (A8)$$

For this to cancel the anomaly in Eq. (A6), we need

$$c_{\text{WZ}}=\frac{C^{(+)}_{\varphi Q}v^2}{12\Lambda^2}. \quad (A9)$$

In our implementation, the contribution from this term can be added together with the $R2$ counterterms, leading to

$$R2_{O^{(+)}_{\varphi Q}}(WW\gamma)=\frac{C^{(+)}_{\varphi Q}e^3 v^2}{96\pi^2 s_W^2 \Lambda^2}\epsilon^{\mu\nu\rho\sigma}(p_{2\sigma}-p_{3\sigma}). \quad (A10)$$

All three other operators can be dealt with in the same way. In practice, we note that this is equivalent to computing the trace by starting from W^+ and W^- respectively, and then taking the average. Finally, we use the same prescription for the WWZ vertex.

References

1 G. Aad et al (ATLAS), Phys. Lett. B, **716**: 1 (2012), arXiv:1207.7214 [hep-ex]
2 S. Chatrchyan et al (CMS), Phys. Lett. B, **716**: 30 (2012), arXiv:1207.7235 [hep-ex]
3 J. Ellis and T. You, JHEP, **03**: 089 (2016), arXiv:1510.04561 [hep-ph]
4 J. Ellis, P. Roloff, V. Sanz, and T. You, JHEP, **05**: 096 (2017), arXiv:1701.04804 [hep-ph]
5 G. Durieux, C. Grojean, J. Gu, and K. Wang, JHEP, **09**: 014 (2017), arXiv:1704.02333 [hep-ph]
6 T. Barklow, K. Fujii, S. Jung, R. Karl, J. List, T. Ogawa, M. E. Peskin, and J. Tian, Phys. Rev. D, **97**: 053003 (2018), arXiv:1708.08912 [hep-ph]
7 T. Barklow, K. Fujii, S. Jung, M. E. Peskin, and J. Tian, Phys. Rev. D, **97**: 053004 (2018), arXiv:1708.09079 [hep-ph]
8 S. Di Vita, G. Durieux, C. Grojean, J. Gu, Z. Liu, G. Panico, M. Riembau, and T. Vantalon, JHEP, **02**: 178 (2018), arXiv:1711.03978 [hep-ph]
9 W. H. Chiu, S. C. Leung, T. Liu, K.-F. Lyu, and L.-T. Wang, JHEP, **05**: 081 (2018), arXiv:1711.04046 [hep-ph]
10 M. McCullough, Phys. Rev. D, **90**: 015001 (2014); Erratum: Phys. Rev. D, **92**(3): 039903 (2015), arXiv:1312.3322 [hep-ph]
11 G. Durieux, M. Perelló, M. Vos, and C. Zhang, arXiv:1807.02121 [hep-ph]
12 E. Vryonidou and C. Zhang, JHEP, **08**: 036 (2018), arXiv:1804.09766 [hep-ph]
13 C. Hartmann and M. Trott, JHEP, **07**: 151 (2015), arXiv:1505.02646 [hep-ph]
14 M. Ghezzi, R. Gomez-Ambrosio, G. Passarino, and S. Uccirati, JHEP, **07**: 175 (2015), arXiv:1505.03706 [hep-ph]
15 C. Hartmann and M. Trott, Phys. Rev. Lett., **115**: 191801 (2015), arXiv:1507.03568 [hep-ph]
16 R. Gauld, B. D. Pecjak, and D. J. Scott, JHEP, **05**: 080 (2016), arXiv:1512.02508 [hep-ph]
17 R. Gauld, B. D. Pecjak, and D. J. Scott, Phys. Rev. D, **94**: 074045 (2016), arXiv:1607.06354 [hep-ph]
18 S. Dawson and P. P. Giardino, Phys. Rev. D, **97**: 093003 (2018), arXiv:1801.01136 [hep-ph]
19 A. Dedes, M. Paraskevas, J. Rosiek, K. Suxho, and L. Trifyllis, JHEP, **08**: 103 (2018), arXiv:1805.00302 [hep-ph]
20 S. Dawson and P. P. Giardino, arXiv:1807.11504 [hep-ph]
21 S. Dawson and A. Ismail, SMEFT Corrections to Z Boson Decays, (2018), arXiv:1808.05948 [hep-ph]
22 S. Weinberg, Phenomenological Lagrangians, Proceedings, Symposium Honoring Julian Schwinger on the Occasion of his 60th Birthday: Los Angeles, California, February 18-19, 1978, Physica A, **96**: 327 (1979)
23 C. N. Leung, S. T. Love, and S. Rao, Z. Phys. C, **31**: 433 (1986)
24 W. Buchmuller and D. Wyler, Nucl. Phys. B, **268**: 621 (1986)
25 C. Degrande, N. Greiner, W. Kilian, O. Mattelaer, H. Mebane, T. Stelzer, S. Willenbrock, and C. Zhang, Annals Phys., **335**:

21 (2013), arXiv:1205.4231 [hep-ph]

26 S. Weinberg, Effective Field Theory, Past and Future, PoS, **CD09**: 001 (2009), arXiv:0908.1964 [hep-th]

27 A. Kobakhidze, N. Liu, L. Wu, and J. Yue, Phys. Rev. D, **95**: 015016 (2017), arXiv:1610.06676 [hep-ph]

28 Z. Liu, I. Low, and L.-T. Wang, Higgs-top interactions at future circular e^+e^- colliders, (2018), arXiv:2018.xxxxx

29 ATLAS Collaboration, ATL-PHYS-PUB-2017-001 (2017)

30 C. Zhang, N. Greiner, and S. Willenbrock, Phys. Rev. D, **86**: 014024 (2012), arXiv:1201.6670 [hep-ph]

31 M. E. Peskin and T. Takeuchi, Phys. Rev. D, **46**: 381 (1992)

32 J. Alwall, R. Frederix, S. Frixione, V. Hirschi, F. Maltoni, O. Mattelaer, H. S. Shao, T. Stelzer, P. Torrielli, and M. Zaro, JHEP, **07**: 079 (2014), arXiv:1405.0301 [hep-ph]

33 O. Mattelaer, Eur. Phys. J. C, **76**: 674 (2016), arXiv:1607.00763 [hep-ph]

34 D. Kreimer, Phys. Lett. B, **237**: 59 (1990)

35 J. G. Korner, D. Kreimer, and K. Schilcher, Z. Phys. C, **54**: 503 (1992)

36 D. Kreimer, The Role of γ_5 in dimensional regularization, (1993), arXiv:hep-ph/9401354

37 A. Pomarol and F. Riva, JHEP, **01**: 151 (2014), arXiv:1308.2803 [hep-ph]

38 T. Corbett, O. J. P. Eboli, J. Gonzalez-Fraile, and M. C. Gonzalez-Garcia, Phys. Rev. Lett., **111**: 011801 (2013), arXiv:1304.1151 [hep-ph]

39 A. Falkowski, M. Gonzalez-Alonso, A. Greljo, and D. Marzocca, Phys. Rev. Lett., **116**: 011801 (2016), arXiv:1508.00581 [hep-ph]

40 J. Wess and B. Zumino, Phys. Lett. B, **37**: 95 (1971)

41 C. Patrignani et al (Particle Data Group), Chin. Phys. C, **40**: 100001 (2016)

42 J. D. Wells and Z. Zhang, JHEP, **01**: 123 (2016), arXiv:1510.08462 [hep-ph]

43 C. Degrande, J. M. Gerard, C. Grojean, F. Maltoni, and G. Servant, JHEP, **07**: 036 (2012); Erratum: JHEP, **03**: 032 (2013), arXiv:1205.1065 [hep-ph]

44 F. Maltoni, E. Vryonidou, and C. Zhang, JHEP, **10**: 123 (2016), arXiv:1607.05330 [hep-ph]

45 CEPC-SPPC Study Group, CEPC-SPPC Preliminary Conceptual Design Report. 1. Physics and Detector (2015)

46 M. Bicer et al (TLEP Design Study Working Group), First Look at the Physics Case of TLEP, Proceedings, 2013 Community Summer Study on the Future of U.S. Particle Physics: Snowmass on the Mississippi (CSS2013): Minneapolis, MN, USA, July 29-August 6, 2013, JHEP, **01**: 164 (2014), arXiv:1308.6176 [hep-ex]

47 M. Benedikt and F. Zimmerman, FCC Week, Amsterdam, 9 Apr 2018

48 M. J. Boland et al (CLICdp, CLIC), Updated baseline for a staged Compact Linear Collider, 10.5170/CERN-2016-004, arXiv:1608.07537 [physics.acc-ph]

49 H. Baer, T. Barklow, K. Fujii, Y. Gao, A. Hoang, S. Kanemura, J. List, H. E. Logan, A. Nomerotski, M. Perelstein, et al, The International Linear Collider Technical Design Report - Volume 2: Physics, arXiv:1306.6352 [hep-ph]

50 A. M. Sirunyan et al (CMS), JHEP, **09**: 051 (2017), arXiv:1701.06228 [hep-ex]

51 B. Schoenrock, E. Drueke, B. Alvarez Gonzalez, and R. Schwienhorst, Proceedings, 2013 Community Summer Study on the Future of U.S. Particle Physics: Snowmass on the Mississippi (CSS2013): Minneapolis, MN, USA, July 29-August 6, 2013, arXiv:1308.6307 [hep-ex]

52 M. Aaboud et al (ATLAS), Eur. Phys. J. C, **77**: 264 (2017), arXiv:1612.02577 [hep-ex]

53 ATLAS Collaboration, Projections for measurements of Higgs boson signal strengths and coupling parameters with the ATLAS detector at a HL-LHC, ATL-PHYS-PUB-2014-016 (2014)

54 E. L. Berger, J. Gao, C. P. Yuan, and H. X. Zhu, Phys. Rev. D, **94**: 071501 (2016), arXiv:1606.08463 [hep-ph]

55 A. Czarnecki, J. G. Korner, and J. H. Piclum, Phys. Rev. D, **81**: 111503 (2010), arXiv:1005.2625 [hep-ph]

56 S. Di Vita, C. Grojean, G. Panico, M. Riembau, and T. Vantalon, JHEP, **09**: 069 (2017), arXiv:1704.01953 [hep-ph]

57 A. Azatov, R. Contino, G. Panico, and M. Son, Phys. Rev. D, **92**: 035001 (2015), arXiv:1502.00539 [hep-ph]

58 M. Beneke, D. Boito, and Y.-M. Wang, JHEP, **11**: 028 (2014), arXiv:1406.1361 [hep-ph]

59 N. Craig, J. Gu, Z. Liu, and K. Wang, JHEP, **03**: 050 (2016), arXiv:1512.06877 [hep-ph]

60 O. Bessidskaia Bylund, F. Maltoni, I. Tsinikos, E. Vryonidou, and C. Zhang, JHEP, **05**: 052 (2016), arXiv:1601.08193 [hep-ph]

61 S. Boselli, R. Hunter, and A. Mitov, Prospects for the determination of the top-quark Yukawa coupling at future e^+e^- colliders, (2018), arXiv:1805.12027 [hep-ph]

62 C. Shen and S.-h. Zhu, Phys. Rev. D, **92**: 094001 (2015), arXiv:1504.05626 [hep-ph]

63 H. Abramowicz et al (CLICdp), Top-Quark Physics at the CLIC Electron-Positron Linear Collider, arXiv:1807.02441 [hep-ex]

64 R. Yonamine, K. Ikematsu, T. Tanabe, K. Fujii, Y. Kiyo, Y. Sumino, and H. Yokoya, Phys. Rev. D, **84**: 014033 (2011), arXiv:1104.5132 [hep-ph]

65 W. A. Bardeen and B. Zumino, Nucl. Phys. B, **244**: 421 (1984)